10.6 OPERATIONAL DETECTION OF "NEAR-SURFACE" RAIN-SNOW BOUNDARIES

Aldo Bellon* and Isztar Zawadzki
J. S. Marshall Radar Observatory, McGill University, Montreal, Canada

1. INTRODUCTION

The timing of the transition from snow to rain and vice versa is of great interest to authorities responsible for the management of transportation networks as well as to every person planning his daily activities. In addition, the remote sensing of areas affected by either rain or snow within the radar coverage, be it near the ground or at higher heights, has a pronounced impact on efforts to improve quantitative precipitation estimates (QPE), not only in the application of a different Z-R relationship but also in the formulation of algorithms seeking to correct measurements made aloft using an average vertical profile of reflectivity (VPR). In fact, events with a possibility of a rain-snow transition are more likely to be associated with a melting layer, or bright band (BB) that is rapidly varying in intensity and height. As a result, the assumption of uniformity of BB characteristics throughout the radar coverage often invoked by VPR corrections schemes as those proposed by Germann and Joss (2002) and Bellon et al. (2007) is not valid in such situations. It is imperative that VPR correction schemes take into account the great variability of the VPR as attempted with some success by Vignal and Krajewski (2001) and Seo et al. (2000). Thus, even in the absence of a change in precipitation phase at the surface, the detection of the varying space-time BB characteristics is of utmost importance in our climatic region in nearly all months of the year. We thus begin this investigation on the detection on rain-snow boundaries with a view of an eventual application to our QPE algorithms as done by Matrosov et al. (2007) with a polarimetric X-band radar.

2. MELTING LAYER DETECTION

Ryshkov and Zrnic (1998) and Zrnic and Ryshkov (1999) have shown that, unlike the situation in rain where both the specific differential phase shift K_{DP} and the differential reflectivity Z_{DR} increase markedly with increasing reflectivity Z, the change of these two polarimetric parameters throughout most of the reflectivity range associated with dry snow is relatively minor. Hence, the discrimination between rain and snow from point measurements is difficult. Fortunately, the transition is often characterized by a zone of mixed phase precipitation. Therefore, as stated by Ryshkov and Zrnic (2003) and again emphasized in Ryshkov et al. (2005), the "rain/snow delineation is contingent on reliable identification of the bright band". While the melting layer can be detected with reflectivity-only measurements as proposed by Gourley and Calvert (2003), the availability of polarimetric radar both simplifies and improves on such algorithms because weaker melting layers may remain relatively 'invisible' with reflectivity-only measurements but exhibit well-defined signatures with polarimetric parameters. The melting layer is characterized by significantly lower ρ_{HV} (cross-correlation coefficient) and higher Z_{DR} values as revealed by Meischer et al. (1991) and Zrnic et al. (1993). This remains true whether the melting layer is horizontally stratified as is usually the case in stratiform precipitation, or vertically elongated in the transition zone between rain and snow at the surface as first demonstrated by Ryshkov and Zrnic (1998). Whereas the typical horizontally stratified BB is less than 0.5 km thick, the vertically elongated melting snow region associated with a sharp frontal boundary may be much deeper, of the order of 1-2 km, Stewart (1992). Thus it becomes an ideal recognizable target for discriminating between rain and snow close to the surface for up to ranges of the order of 100 km from the radar. Brandes and Ikeda (2004) have implemented a successful algorithm for estimating freezing level heights but it is reliant on the linear depolarization ratio (LDR) parameter that is not available with our radar system (nor with the WSR-88D radars in the US). Scharfenber and Maxwell (2003) and Miller and Scharfenber (2003) discuss the operational benefits of knowing the exact height of the 0° C height for winter storms. But while the likelihood of such occurrences remains relatively uncommon in Oklahoma, the latitude of Montreal in the middle of the westerly jet throughout most of the year places our region into a higher probability of several such occurrences any time between mid-November to mid-April.

3. THE McGILL POLARIMETRIC RADAR

From its very beginnings in the early 70's, the McGill S-band radar has always been operated in a fast scanning mode (6 rpm) for real-time weather surveillance, (Marshall and Ballantyne, 1975), achieving a 24-elevation reflectivity volume scan every 5 minutes to which a radial velocity volume scan was added when it was dopplerized in 1993. The implementation of a dual polarization capability in the year 2000 achieved with the simultaneous transmission and reception of horizontally and vertically polarized waves provided three additional

*Corresponding author address: Aldo Bellon, J. S. Marshall Radar Observatory, P. O. Box 198, Macdonald Campus, Ste-Anne-de-Bellevue, QC, Canada.
H9X 3V9 E-mail: aldo.bellon@mcgill.ca

volume scans consisting of the differential reflectivity Z_{DR}, (10 x log(Z_H/Z_v)), the differential phase Θ_{DP}, (from which the differential phase shift K_{DP} can be derived), and the cross-correlation coefficient ρ_{HV} between the two copolar components of the returned echo. All these volume scans are archived with the same frequency (every 5 minutes) and resolution (1 km by 1 degree for 24 elevation angles). While our efforts to use K_{DP} for directly estimating rainfall rates were not successful on account of the predominance of light rainfall affecting our region (Lee, 2006), the polarization capability has indirectly helped in improving rainfall estimates by permitting a more effective removal of non-meteorological echoes through target identification (Zawadzki et al. 2001). Particle type classification on a pixel-by-pixel basis has been achieved using a fuzzy logic approach as described by Vivekanandan et al. (1999) and modified for our region. While only a few elevation angles would be sufficient to detect the "near-surface" rain-snow switch, the availability of 3-D polarimetric data from 24 scans every 5 minutes has the potential advantage of being better able to identify the type of precipitation on either side of the transition zone. Given, as stated earlier, that the polarimetric characteristics of light rain and of dry snow are similar for light to moderate reflectivities, then an additional goal is to investigate whether an examination of the 3-D structure of these parameters can at least indirectly assume a rain regime through the identification of a BB aloft. An attempt will also be made to assume snowfall at the ground if, given the absence of such a BB aloft, the reflectivity gradient immediately above the lowest elevation angle is characteristic of typical snow profiles of gradually decreasing reflectivity with height. Our scheme is not yet finalized as more experience is gained from the analysis of additional cases. What we are presenting here is thus "work in progress".

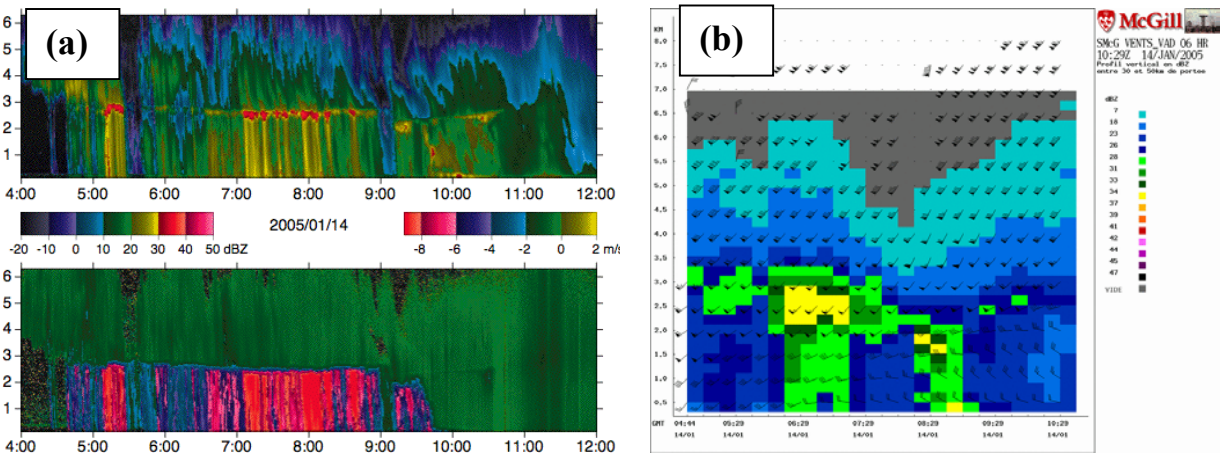

Fig. 1 *a): Reflectivity and vertical velocity profiles derived from an X-band vertically pointing radar from 0400 to 1200 UTC on 14 January 2005, and (b), the vertical profile of reflectivity from the McGill scanning radar obtained by averaging in azimuth all the data between 30 and 50 km. The time interval of the latter is from 0430 to 1030 UTC. The derived VAD winds have been superimposed. During this period, the X-band radar was collocated with the scanning radar.*

4. SELECTION OF EVENTS

The selection of cases pertinent to our analysis is best achieved by examining the reflectivity, and especially, the terminal fall velocity data, from a UHF wind profiler, (Rogers and Brown, 1997), situated on the campus of McGill University, 30 km east of our scanning radar site or from an X-band vertically pointing radar, Fabry and Zawadzki (1995), that has since then been dopplerized. We have catalogued about 25 events that have occurred within the past 6 years, with various degrees of "sharpness" in the precipitation phase change. A well-defined wet-snow region moving over a significant range of the radar coverage has been observed for about 2/3 of the selected events using the existing reflectivity, Z_{DR} and ρ_{HV} PPI and CAPPI maps already available with our radar display system. So far, we have applied the proposed automatic "near-surface" rain-snow detection scheme to only a handful (~5) of these events, which we have used to help formulate and improve its various algorithms. In this manuscript, we concentrate on the event of 14 January 2005 to describe in some detail our observations, procedure, and results for automatically detecting and monitoring the motion of "near-surface" rain-snow boundaries and for classifying surface precipitation type on either sides of such boundary. Manuscript size constraints prevent us from presenting maps at a greater frequency in time and space. A more complete set, as well as those from other events not shown here, can be viewed online: http://132.206.43.159/~aldo/rsbd. As seen in Fig. 1a, the fall velocity of hydrometeors is a better indication of the type of precipitation at the ground than the reflectivity measurements. Velocities > 4 m/s indicate rain while snow is characterized by velocities < 1.5 or 2 m/s, with mixed or rimed particles occupying the intervening gap. The top of the melting layer is seen to

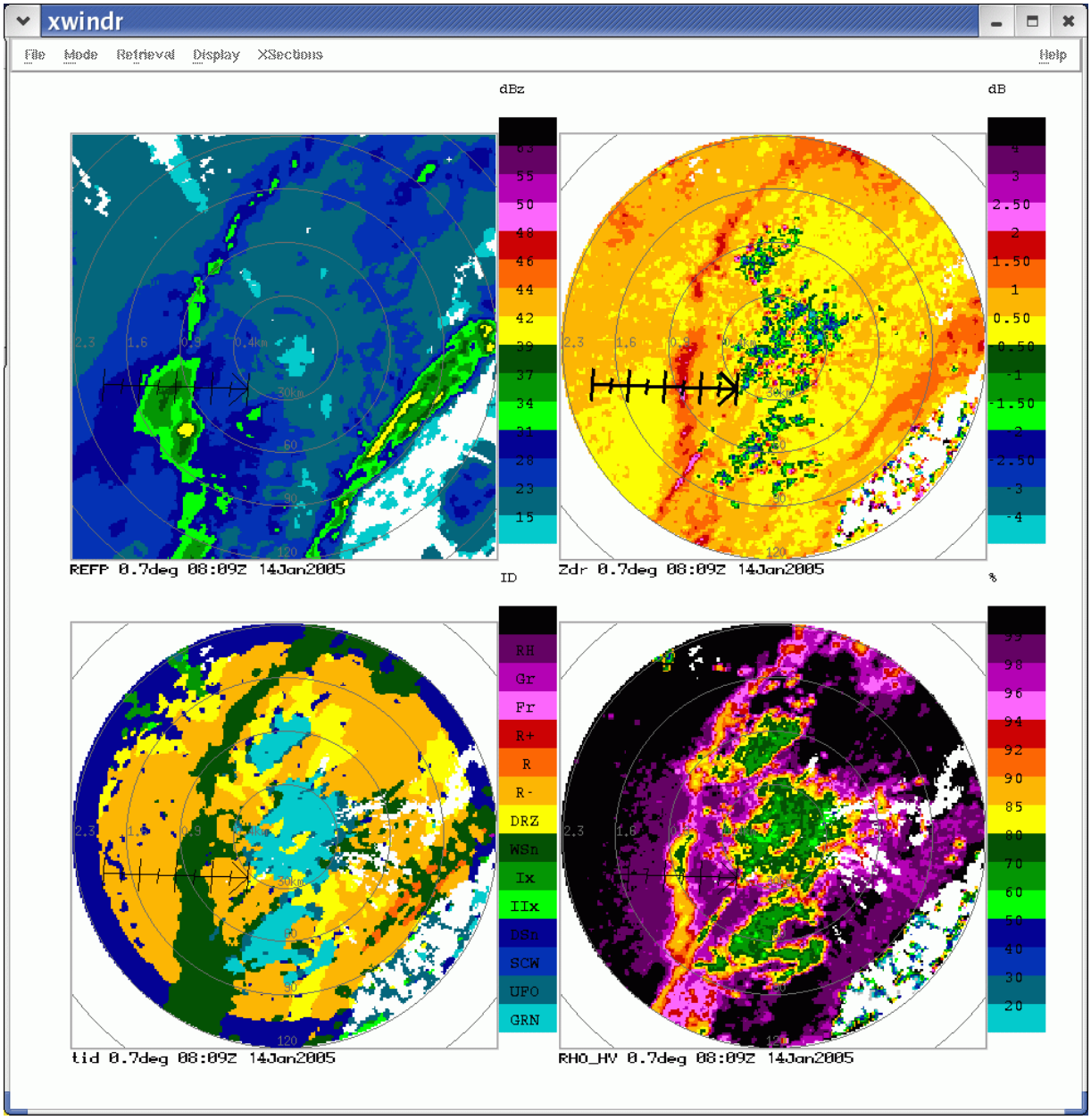

Fig. 2: *Reflectivity, Z_{dr}, PID (particle identification) and ρ_{hv} PPIs at an elevation angle of 0.7 degrees at 8:09 UTC on 14 January 2005. The symbols GRN, DSn, WSn, Ix, R-, DRZ identify ground clutter, dry snow, wet snow, ice crystals, light rain and drizzle respectively. The existing PID algorithm at that time could not differentiate between light rain and snow and relied on temperature profile forecasts which can be in error along strong frontal boundaries. Without an examination of the 3-D structure of the data, light rain is assumed on both sides of the transition zone correctly identified as WSn. Range rings are 30 km apart to a maximum range of 120 km. The arrow indicates the path of the vertical cross-sections shown in Fig. 3.*

be between 2.8 and 2.5km till about 0900 UTC, - unusually high for the coldest time of the year in our climate - but then drops sharply during the next hour. The change-over from rain to frozen particles occurs during this interval with completely dry snow observed at the ground at ~0950 UTC. Note the remnants of a BB aloft until nearly 1100 UTC, but the fall velocities below it clearly characterize the particles as snow. The same observation could not be made from the UHF data located 30 km away (not shown) where a

similar BB aloft is the source of partially melted particles at the surface with fall velocities between 1.5 and 3 m/s, thus underlining the complexity of the precipitation near rain-snow boundaries. Even though the spatial and temporal resolution of the scanning radar is generally an order of magnitude less than that of the X-band profiler, the sudden drop of the melting layer is also adequately depicted in Fig. 1b showing the profile of reflectivity derived over the 30-50 km range interval. The low level VAD winds veer from SW to NW as the cold air reaches the ground behind the frontal boundary. Such deep rain-snow transition extending for over 2 km above the earth's surface are expected to be well captured by our proposed scheme. In other events, the rain-snow boundary slopes with height in a much more gradual manner, or fails to descend below the lowest 500 m of the atmosphere. We must accept the fact that the latter will likely constitute the "false alarms" of our radar-based automatic scheme when verified with actual surface observations, even without the "nuisance" of our nearby ground clutter. As is the case on the profiler data, we see in Fig. 1b the remnants of a BB aloft after the cold front passage. Its presence will unfortunately prevent us from deducing the presence of snow at the surface immediately after the cold front using our scanning radar, even though the velocities shown in Fig. 1a imply that the precipitation reaching the ground after ~0900 UTC is mainly of the frozen variety.

5. POLARIMETRIC DATA

5.1 Polarimetric PPIs

In Fig. 2 we provide examples of polarimetric data from our operational scanning radar as observed at 809 UTC 14 January 2005 when the frontal zone responsible for the rain/snow transition seen on Fig. 1 was ~60 km west of the radar site. The low elevation PPIs at 0.7 degrees indicate a narrow north-south wet-snow zone close to the surface as deduced from the combination of Z_{DR} measurements > 1.0 db with ρ_{HV} < ~0.92. This wet-snow region is evident even in the reflectivity PPI, although such confirmation is usually difficult to establish because of the known large horizontal variability of reflectivity measurements. The results of the pixel-by-pixel particle identification algorithm based on membership functions proposed by Vivekanandan et al. (1999) shown in the PID PPI does properly identify this region as wet-snow but, as anticipated by Zrnic and Ryshkov (1999), cannot distinguish between the light rain ahead of the front from the probably snow or at least partially frozen precipitation behind it. The algorithm relied instead on forecasts from the Rapid Update Cycle (RUC-2) model of temperature profiles at one location, the radar site, for deciding on the nature of targets having a similar probability of being light rain or snow from a polarimetric perspective. Consequently, dry snow is indicated only at all ranges beyond ~110 km, at a height corresponding to the 0° C isotherm as predicted by the RUC-2 model for the radar site. Even if forecasts were obtained at a finer spatial resolution, the expected model phase errors cannot guarantee the needed accuracy of the order of tens of kilometers, especially in such rapidly evolving frontal situations. The animation of similar images accessible from our Web site noted in section 4 vividly shows the movement of the wet-snow region across the radar coverage from the edge of the map in the NW at ~0700 UTC to the eastern part of the map at 1000 UTC. It is clear from many aspects that such a feature is not associated with a horizontally stratified melting layer as is usually the case in stratiform rainfall events. Upon an animation with PPI images of the latter situation, the BB would appear as essentially a nearly stationary concentric ring at a range corresponding to a height slightly below that of the 0°C isotherm, subject to only minor height and intensity variations. The cross-sections of polarimetric parameters along the path indicated by the arrow in Fig. 2 and presented in Fig. 3 well depict the more complex 3-D structure of the melting layer near strong frontal boundaries. The change from a horizontally stratified melting layer slightly above 2 km ahead of the front to a vertically elongated wet snow zone extending downwards to the lowest height seen by radar, and with no BB signature behind such feature, leads to a convincing argument for a rain-snow boundary. In fact, these images are very similar to the schematic representation of the microphysical processes near a transition zone as sketched in Fig. 6 by Stewart (1992). However, they also underline the basic limitation for the remote sensing of conditions at the surface, because, even in the absence of ground clutter as in the example of Fig. 3, we can truly make assertions about the type of precipitation for only the heights corresponding to the lowest elevation angle which, even at moderate ranges of ~60 km, can be higher than 0.5 km.

5.2 Melting Index (MIX) PPIs

In order to aid in the decision-making process of whether a particular pixel of the maps in Fig. 2 is affected by a BB that is only aloft, or by one that is reaching the ground, or by no BB at all, it is useful to assign a "melting index" that is based on the polarimetric (Z_{DR} and ρ_{HV}) measurements at all the elevation angles above that pixel. We first assume a selectable Z_{DR} and ρ_{HV} range of values associated with wet-snow. Ryshkov and Zrnic (1998) report ρ_{HV} point values as low as 0.5 while Brandes and Ikeda (2004) model a BB profile with ρ_{HV} minimum values above 0.9. According to Matrosov et al. (2007), and from the experience with our own radar, the range in ρ_{HV} magnitudes associated with a bright band is about 0.7 <ρ_{HV} < 0.95, with values > 0.95 being associated with rain, and those < 0.7 being possibly of a non-meteorological nature such a ground clutter, chaff or biological scatterers, (Zrnic and Ryshkov, 1999). A reasonable range in Z_{DR} measurements associated with wet-snow is 0.7 < Z_{DR} < 2.0. In our algorithm, all variables are user-selectable so that sensitivity tests

can be performed with reasonable variations of these variables. This includes, for example, the degree of smoothing applied to the 3-D polarimetric data in order to reduce noise, a typical choice being 3 km by 3 degrees. In order to avoid known biases in polarimetric measurements, Ryshkov et al. (2005) recommend that the resulting combination of Z_{DR} and ρ_{HV} measurements be associated with a signal-to-noise ratio (SNR) of at least 5 to 10 db. Moreover, since the peak of the melting layer may not be properly sampled aloft for every pixel at the surface on account of geometrical considerations, (Sanchez-Diezma et al. 2000), a search is performed for the smoothed lowest ρ_{HV} and highest Z_{DR} in a selectable (3 x 3) polar neighborhood around that pixel. We then limit the smoothed ρ_{HV} and Z_{DR} values to their lower (0.60 to 0.80) or upper (2.0 to 3.0 db) wet-snow limit respectively to derive a range of possible wet-snow measurements:

(Z_{DR} range) = (Z_{DR} up – Z_{DR} low) and

(ρ_{HV} range) = (ρ_{HV} up - ρ_{HV} low)

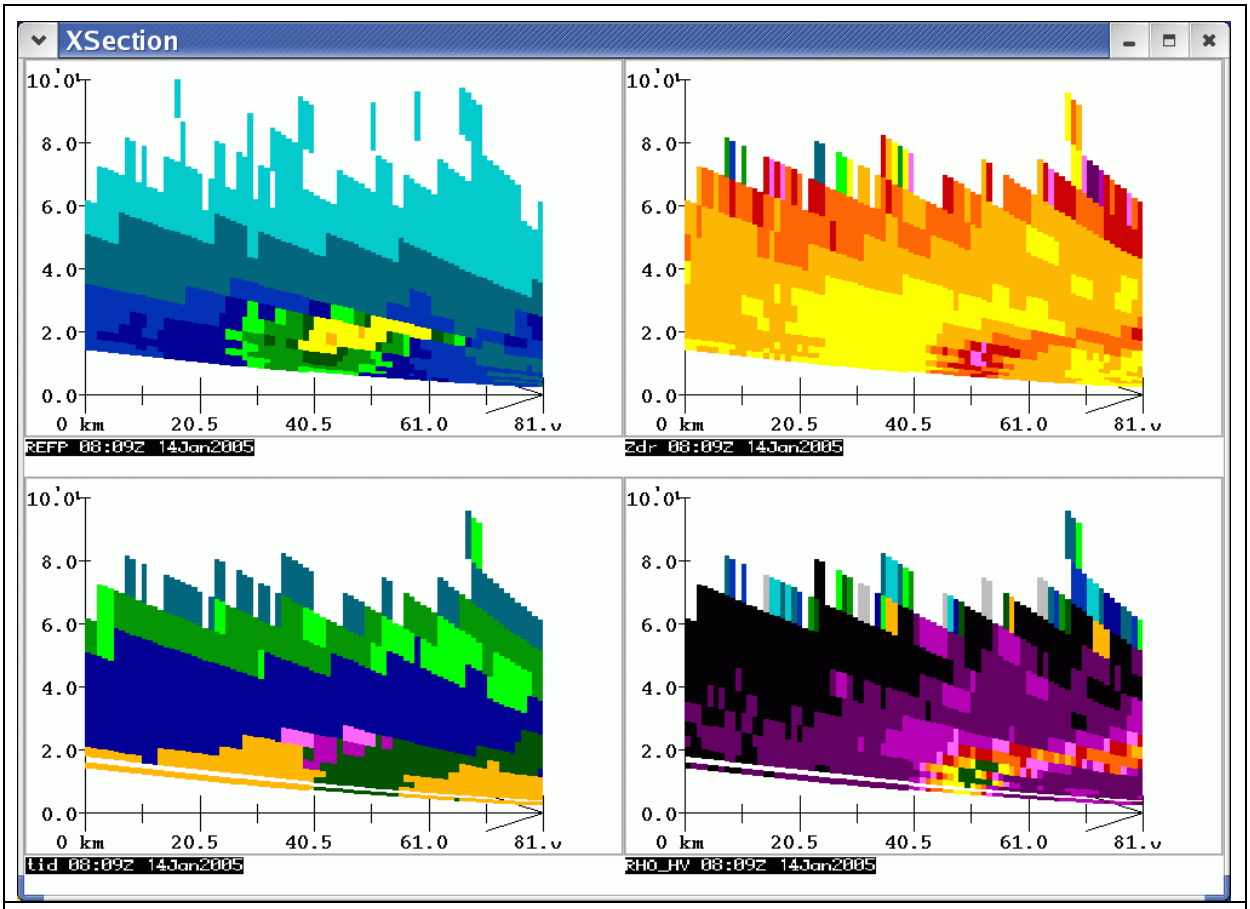

***Fig. 3**: Vertical cross-section of reflectivity, Z_{DR} , PID, and ρ_{HV} across the rain-snow transition zone indicated by the arrow in Fig. 2 as obtained from the 3-D data of the rapid scanning McGill polarimetric radar. The legends are as in Fig. 2. The change from a horizontally stratified BB to a vertical rain-snow boundary reaching the lowest elevation angle (surface) is well illustrated in all the 4 parameters. The indicated distances in km are measured from the beginning of the path.*

The melting index *MIX* can then be expressed as the product of the ρ_{HV} and Z_{DR} contributions as follows:

$MIX = 100 \{Z_{DR}\text{ (contr) } \rho_{HV}\text{ (contr)}\}$ where

$Z_{DR}\text{ (contr)} = \{(Z_{DR} - Z_{DR}\text{ low})/(Z_{DR}\text{ range})\}^{(1/p)}$ and

$\rho_{HV}\text{ (contr)} = \{(\rho_{HV}\text{ up} - \rho_{HV})/(\rho_{HV}\text{ range})\}^{(1/p}$

Unlike a formulation where *MIX* is taken as the weighted sum of the two contributions, a high contribution from one of the parameters can be diminished by a low contribution from the other. If the ρ_{HV} and Z_{DR} values are each in the middle their respective range, then *MIX* = 25, 50, 63 and 71% for *p* = 1, 2, 3 and 4 respectively. Since we judge the likelihood of wet-snow to be fairly high under such a situation, we are inclined to select at least *p* = 3. As it

turned out, this choice merely provides plausible magnitudes for displays of *MIX* PPIs as shown in Fig. 4, because, in our subsequent analysis, no *MIX* threshold was considered necessary, that is, a pair of ρ_{HV} and Z_{DR} measurements within their respective selected range implies a wet-snow pixel. Fig. 4a and b provide the *MIX* parameter at 0809 UTC at two relevant elevation angles, (#1 at 0.5 degrees and #8 at 2.2 degrees). The *MIX* values seen in (a) 60 km west of the radar and extending north and south are obviously associated with the "near-surface" rain-snow boundary. There is therefore no corresponding wet-snow feature at similar ranges towards the east where rain prevails. A BB aloft is only seen in (b) although the asymmetric characteristics of the BB signature at an elevation angle of 2.2 degrees hints at the complexity of the situation, with the possible presence of warm rain in the south-east failing to provide the expected BB signal. Warm rain is in fact suspected from the UHF profiles at 0800 UTC (not shown). The non-uniformity of the melting layer as viewed with the *MIX* parameter is further illustrated in (c) taken at 0844 UTC at an elevation angle of 3.4 degrees. The usual "ring" around the radar associated with a typical melting layer in uniform conditions has become a "D-shaped" feature that indicates rain only in the east and a rain-snow boundary that is in the process of crossing the radar site. Again, "spatial" animations of *MIX* PPIs consisting of a greater number of elevation angles for a given time as well as temporal animations can be viewed from our Web site.

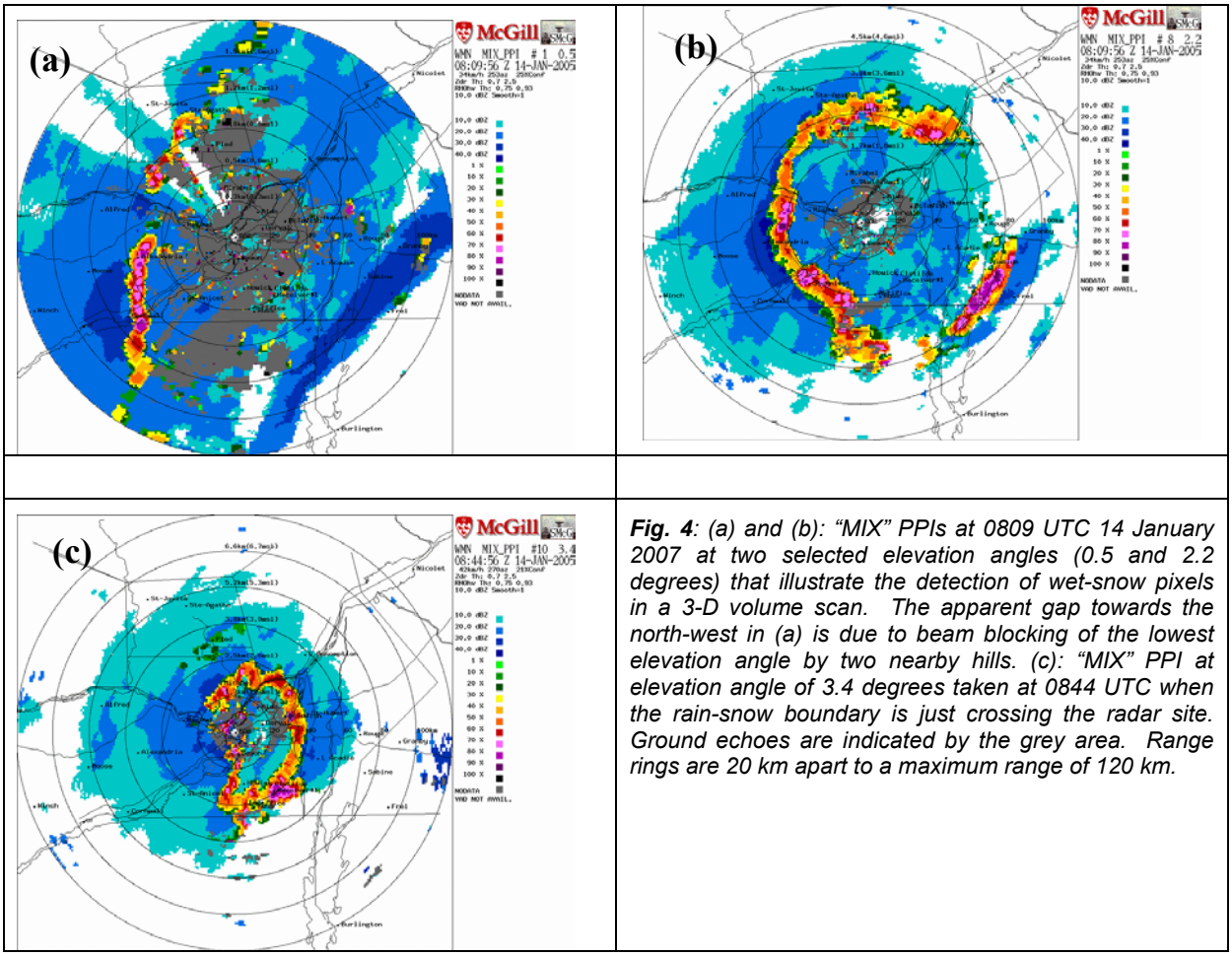

***Fig. 4**: (a) and (b): "MIX" PPIs at 0809 UTC 14 January 2007 at two selected elevation angles (0.5 and 2.2 degrees) that illustrate the detection of wet-snow pixels in a 3-D volume scan. The apparent gap towards the north-west in (a) is due to beam blocking of the lowest elevation angle by two nearby hills. (c): "MIX" PPI at elevation angle of 3.4 degrees taken at 0844 UTC when the rain-snow boundary is just crossing the radar site. Ground echoes are indicated by the grey area. Range rings are 20 km apart to a maximum range of 120 km.*

5.3 Rain-Snow Boundary Maps

After computing the MIX index at all the 24 elevation angles, some simple rules can be formulated in order to establish whether any wet-snow pixels detected above a given point constitute a BB aloft or one that is reaching the ground. Thus, after interpolating in height any small gaps in the detection of wet-snow pixels, a melting layer that exceeds a user-selectable thickness (0.1 – 0.5 km) with a bottom that is within a selectable height threshold (0.1 – 0.4 km) from either the lowest elevation angle or from the highest ground echo while remaining less than say 1 km from the earth's surface is judged to be a "near-surface" rain-snow boundary. Otherwise, any BB that satisfies the thickness threshold is considered to be only aloft, and thus associated with stratiform rainfall at the surface. This two-category classification leaves

large portions of the map with “undetermined” profiles as seen by the green area in Fig. 6a. Given the possibility of some convection or of “warm rain”, the lack of some wet-snow pixels above a given point does not automatically imply a “dry snow” profile. We have thus derived “local” vertical profiles of reflectivity (LVPR) with the hope that averaging over a larger area may help identify a particular profile not detectable from point measurements. Averaging is done in Z units and ground clutter is obviously excluded. The typical averaging area is 20 km in range by 20 degrees in azimuth derived at every 10 km in range, thus allowing some overlapping in the radial direction. As can be deduced from Fig. 5, the 20-degree azimuth width has been maintained beyond 60 km, but is adjusted at closer ranges so as to maintain an approximate 20 km by 20 km size. The azimuth width is thus 40 degrees at a range of 30 km, etc. There is no azimuth overlapping and the profile is computed up to a maximum height of 8 km at resolution of 0.2 km for a maximum of 40 “layers”. In Fig. 5, the bottom left-hand corner of each LVPR is plotted at the centre of the averaging area. In order to avoid the mutual “hiding” of profiles occurring mainly along the north-south sectors of the map, we have slightly staggered their exact position. The display of each profile is terminated at echo top up to a maximum height of 6 km. Black pixels on the left-hand side of each profile are provided at every kilometer in height.

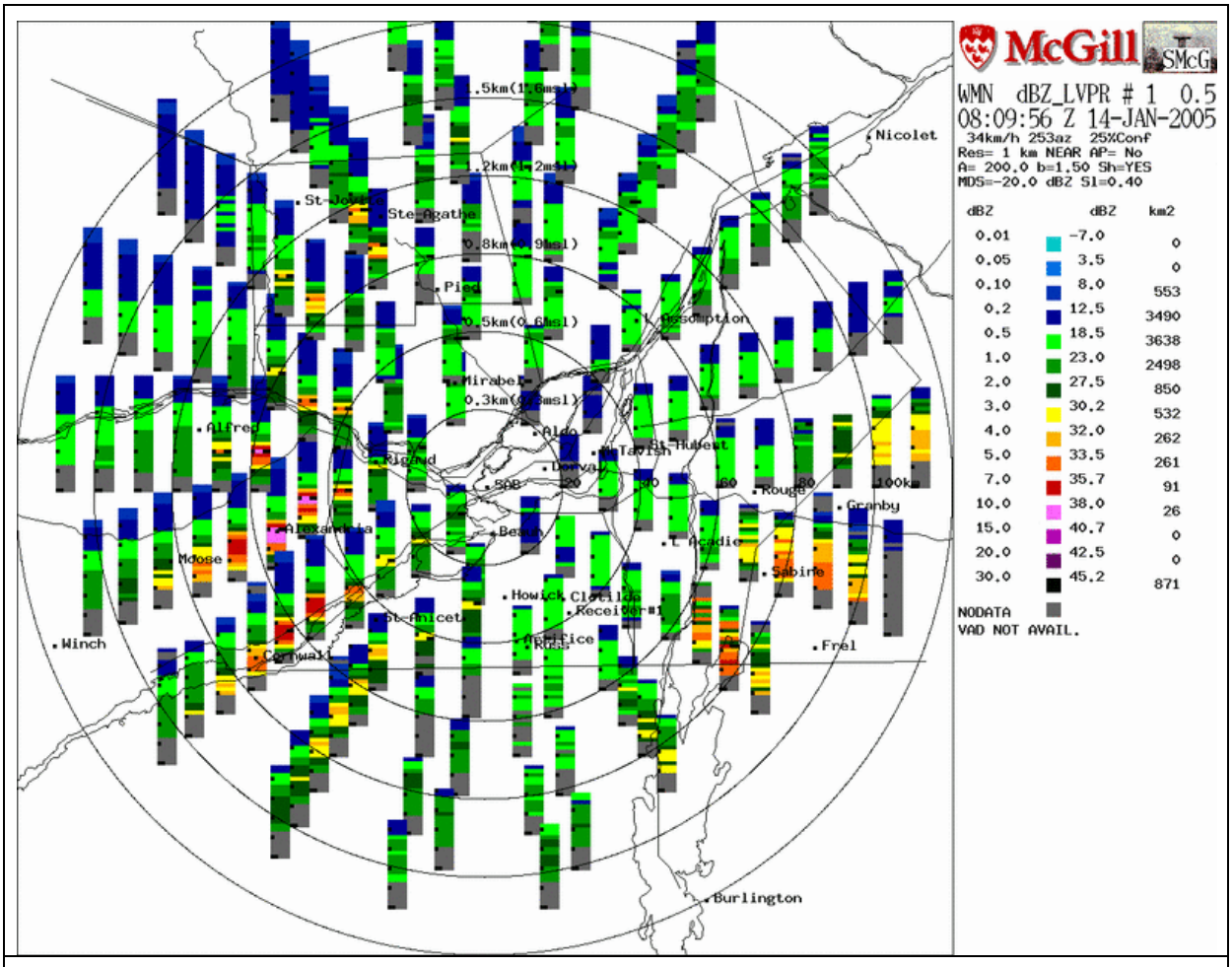

Fig. 5*: Map of LVPRs (local vertical profiles of reflectivity) at 0809 UTC 14 January 2005. Range rings are 20 km apart up to a maximum range of 120 km. Refer to text for details.*

The remarkable aspect of this display is the high variability of the LVPRs in space (and time when viewed in animation), which as briefly discussed in the introduction, has profound implications when correcting QPE with one or a few average VPRs and then assuming homogeneity of rainfall fields up to the farther ranges of the radar coverage. It is apparent that this assumption is not valid when precipitation is associated with a sharp baroclinic zone. For our present purpose, we will use these LVPRs to search for any BB aloft that may have escaped detection with the point polarimetric measurements, and, especially, to infer a snow profile for the undetermined regions of

Fig. 6a. Fig. 5 reveals that the LVPRs 30 to 50 km west of the radar display an obvious BB signature at a height of ~2 km, those in the WSW beyond 60 km near Cornwall show a BB near the ground while the BB remain aloft at all ranges for the LVPRs along the next "row" in the SSW direction. The LVPRs at far ranges in the NW seem to imply a gradually decreasing reflectivity with height usually associated with snow, but a similar observation could be made for some LVPRs ~40 km east of the radar. In the latter case though, the lower height of their echo tops which coincides with the height of the BB of neighboring LVPRs, would instead suggest a warm rain mechanism. (This check was not coded at the moment of writing this manuscript but we intend to do so in an updated version of our algorithm). Even though we have also derived ρ_{HV} and Z_{DR} LVPRs (not shown), so far, we have used only the reflectivity LVPRs for our stated purpose. A BB aloft is assumed if a reflectivity peak above a selectable threshold is found above the lowest (or two lowest) layers of the profile. This peak must satisfy a selectable, but then range-modified, total drop in the rain and snow at a height difference that is a function of the peak intensity. However, the detection of a snow profile from reflectivity-only measurements is more problematic. A simple assumption considers snow at the surface when the peak reflectivity is found in the lowest (or two lowest) layers of the profile and the reflectivity drop above is not sufficiently large to be associated with a low BB. Otherwise, after failing to detect a BB aloft, the gradient of reflectivity just above the lowest layers of the profile is computed. Snow at the surface is then assumed if this gradient satisfies a selectable threshold, (at least 1 to 2 dBZ/km). The encounter of a positive gradient exceeding a selectable magnitude, (~4 dBZ/km), is sufficient to negate any snow profile. The result of adding the LVPR analysis to the initial polarimetric-only classification of Fig. 6a is shown in Fig. 6b.

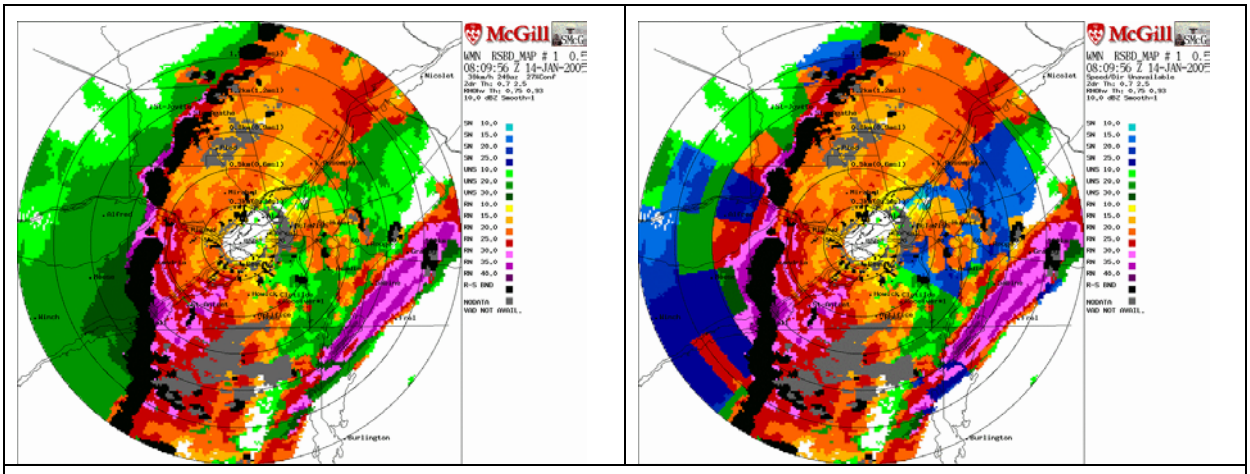

Fig. 6 *(a): Rain-snow boundary map obtained solely from the 3-D MIX analysis at 0809 UTC 14 January 2005 indicating the "near-surface" rain-snow transition zone in black and the area where the precipitation is judged to be in the form of rain (warm colors) due to the presence of a BB aloft. Green colors indicate that no BB has been detected using the point polarimetric measurements and thus imply an "undetermined" precipitation type. (b) As in (a) but after adding the information obtained from the LVPRs of Fig. 5. Blue colors now identify the likely presence snow at the surface, while the "undetermined" profiles after both the "MIX" and LVPR analyses remain green. The different shades within each color group are related to the reflectivity at a CAPPI height of 1.5 km. Ground clutter is grey.*

The LVPR analysis can only affect the green areas of Fig. 6a, that is, the pixels in the "rain" and the "transition zone" are not allowed to change to a snow profile. Since the profile classification is taken from the LVPR nearest a given pixel, the result is necessarily molded by the shape of the LVPR sectors. While it may not be esthetically pleasing, it nonetheless satisfies a useful purpose during the development stage of the algorithm. Eventually, the LVPRs could conceivable be computed at a higher spatial density while maintaining their typical size of (20 km by 20 km). We notice from Fig. 6b that the averaging has enabled the detection of a few additional rain areas just behind the rain-snow boundary. They are probably low BB and may justify an additional category in our display. Some snow profiles have been identified farther behind the rain-snow boundary but perhaps not as many as was expected (or hoped for when introducing the LVPR analysis). A careful examination of the actual magnitudes of the reflectivity profiles west of the boundary has revealed that the reflectivity is essentially constant in the lowest layers and thus failed the test for a predominantly negative gradient immediately above the surface. Conversely, the same criteria has declared as snow profiles some

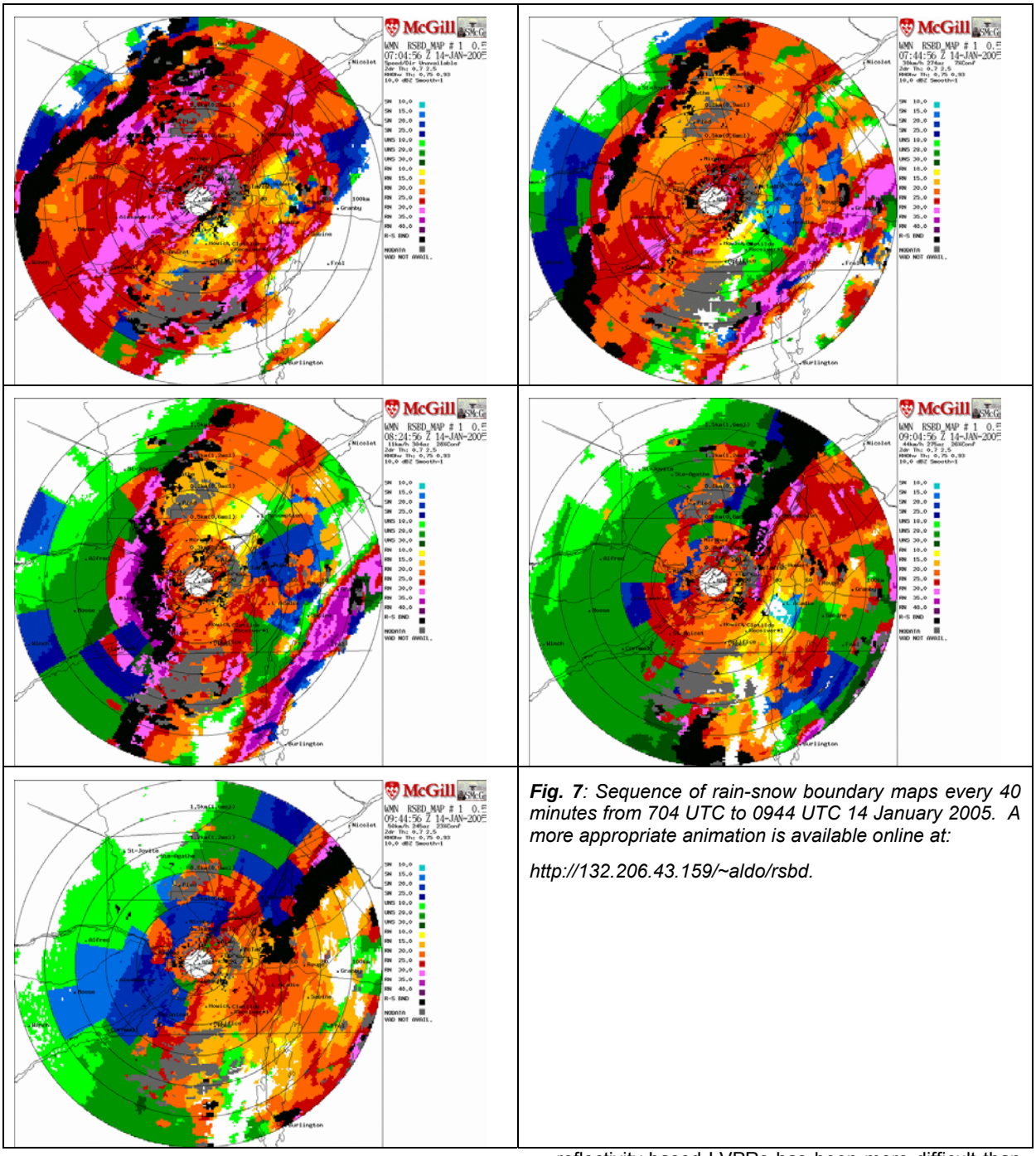

***Fig. 7**: Sequence of rain-snow boundary maps every 40 minutes from 704 UTC to 0944 UTC 14 January 2005. A more appropriate animation is available online at:*

http://132.206.43.159/~aldo/rsbd.

LVPRs just east of the radar that, as we have already noted, may instead be due to a warm rain process. The proposed modifications involving the echo top and the 0°C height should prevent these erroneous classifications. The partial BB seen in Fig. 1 between 0900 and 1050 UTC is likely also responsible for preventing the detection of additional snow profiles behind the frontal boundary. This can best be seen in the last two maps of the sequence of images of Fig. 7.). While the simple detection of snow profiles from reflectivity-based LVPRs has been more difficult than anticipated, we can nevertheless state that the present technique manages to separate the mainly rain region from an "undetermined" or "snow' region with a well-defined "near-surface" rain-snow boundary that remains detectable as it moves across the radar coverage over an extended period of about three hours. We can then rely on reasonable assumptions on the part of the forecasters in deducing the true nature of the unknown type of precipitation at the surface indicated by these maps. Other detailed

information, as exemplified by the maps of the BB bottom and BB thickness in Fig. 8, provides further evidence to the argument for mainly snow behind the transition zone. Having developed a procedure that identifies BB aloft from polarimetry and LVPRs, and after the proposed improvements regarding the warm rain process and convection, one may be inclined to declare as snow the remaining region of precipitation. Such a simple solution, as well as other aspects of our present technique, needs to be evaluated against actual surface observations. We conclude by showing in Fig. 9 only one map of a sequence in which a distinct rain-zone transition zone remained within radar coverage for an extended period of 22 hours, (0600 UTC 8 April to 0400 UTC 9 April 2000). It was associated with a well-organized east-coast low pressure system with precipitation in the Montreal area beginning as snow at ~0500 UTC, then as rain at ~0900 and back to snow around midnight. Beginning at ~0600 UTC, our procedure delineates an east-west oriented transition zone moving from the south and crossing the Montreal area just before 1100 UTC, nearly 2 hours after the apparent switch to rain at the surface according to UHF data. This discrepancy is due to the shallow nature (< 400 m) of the warm rain close to the surface, a phenomenon which is not expected to be well captured by radar. This line then slowed its northward progression and remained nearly stationary at a range of about 80 km until about 1800 UTC while slowly changing its orientation. Then it began to swing counterclockwise and to assume a mainly north-south alignment as it started to be advected eastward following the motion of the low pressure system out of the region, bringing another change in precipitation at the surface, from rain to snow across the radar coverage. The time of 2300 UTC of Fig. 9 corresponds to this latter phase of the storm passage. We point out that, as can be seen in this example, and actually throughout the entire 22-hour event, the LVPR analysis resulted into a larger number of detection of snow profiles than was the case with the event of 14 January 2005.

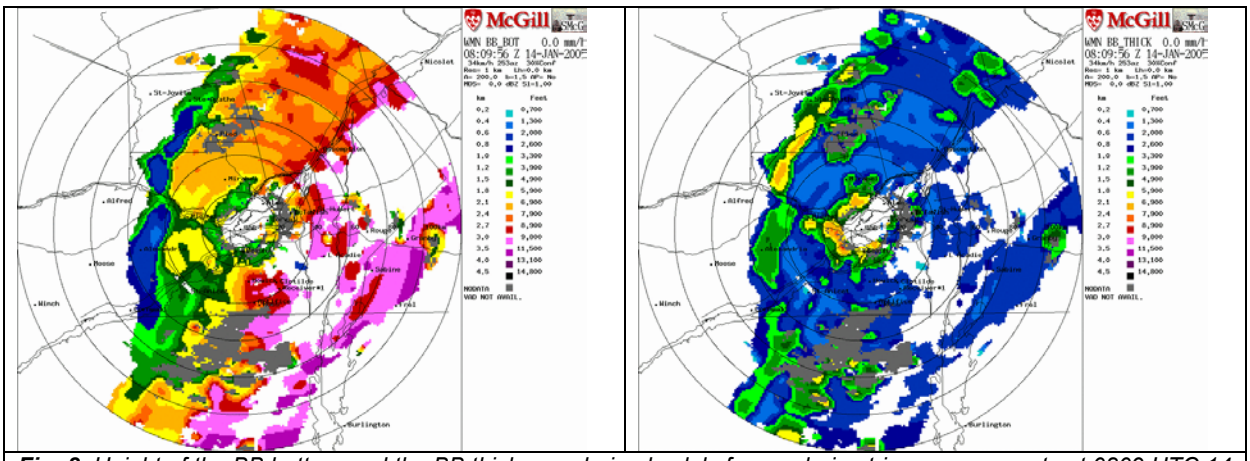

***Fig. 8**: Height of the BB bottom and the BB thickness derived solely from polarimetric measurements at 0809 UTC 14 January 2005. The addition of the BB top map would have exceeded size constraints but may be viewed online.*

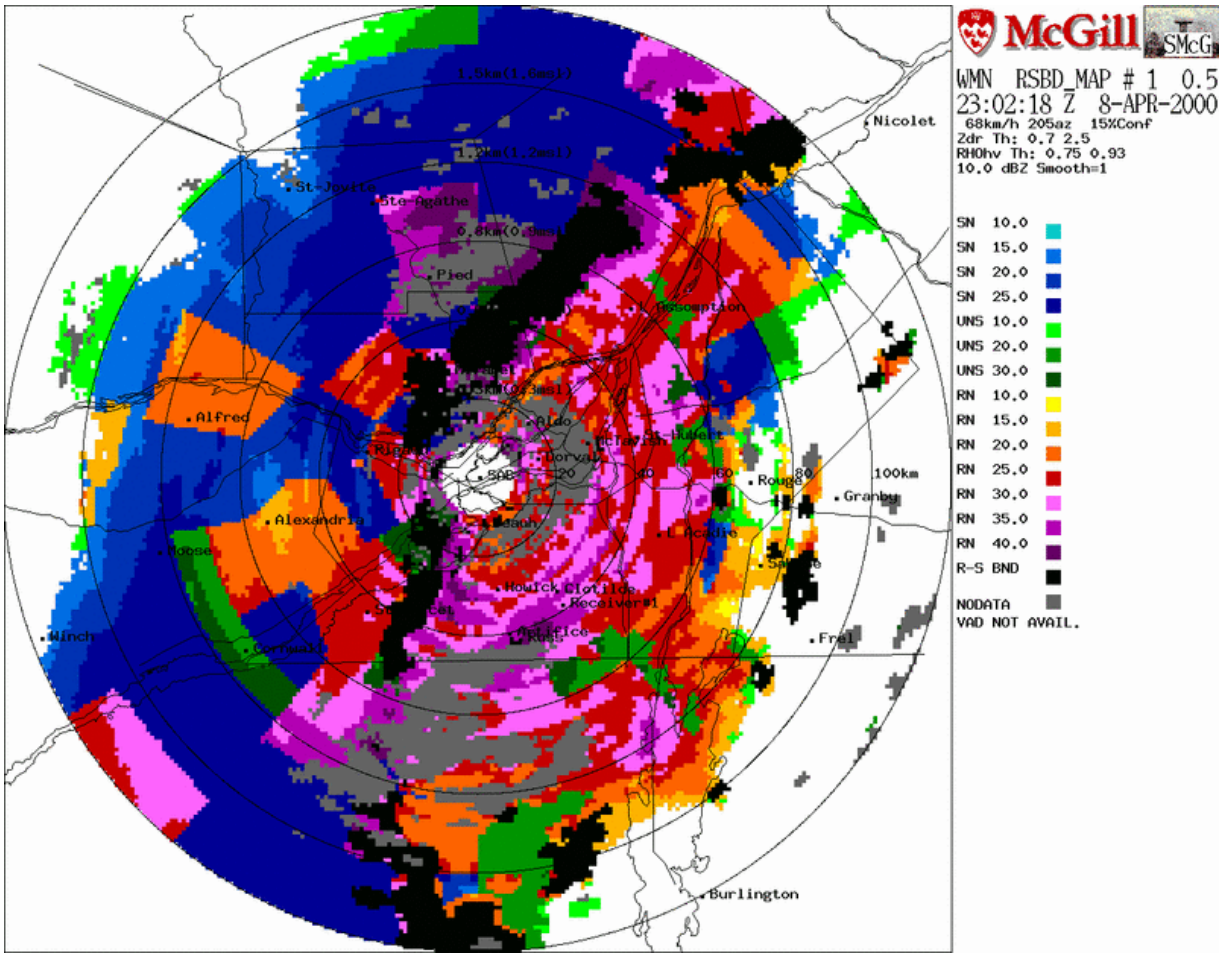

***Fig. 9**: Rain-snow boundary map at 2302 UTC 8 April 2000. For this event, a rain-snow boundary has remained detectable within radar range for 22 hours (0600 UTC on the 8th to 0400 UTC on the 9th)*

6. CONCLUSIONS

The McGill polarimetric radar is ideally situated to monitor the several episodes per year of a rain/snow transition that can affect the Montreal region during the winter season typically extending from mid-November to mid-April. However, any radar-based algorithm seeking to identify "near-surface" features is constrained by the increasing height with range of the lowest elevation angle. A rain/snow transition that is confined to lowest 0.5 km of the atmosphere will essentially escape detection because of the extensive ground clutter of our S-band data at the very close ranges. It is thus necessary that the sharp transition zone characterized by higher Z_{DR} and lower ρ_{HV} extend over nearly a kilometer from the surface. While recognizing this fundamental limitation, we can still claim some success in monitoring for several hours and over distances of the order of 100 km not only the motion of rain-snow boundaries across the radar coverage but also the identification of the accompanying rain/snow regions. The few events analyzed so far indicate that the rain region is easier to confirm because the presence of a BB aloft can be easily be deduced from 3-D polarimetric data or from local vertical profiles of reflectivity "LVPRs". The availability of a 3-D polarimetric scan consisting of 24 scans every 5 minutes is of utmost importance in this classification. The confirmation of a snow region indirectly from the absence of a BB and from the reflectivity decrease with height near the surface is more problematical as expected. General trends are observed in the polarimetric variables (Z_{DR} and ρ_{HV}) during a frontal passage in the rain and snow regions but a more robust and automatic distinction is limited by considerable overlapping of those variables. We are developing a procedure for distinguishing a warm rain profile devoid of a BB from a snow profile. The planned comparison of the echo top of such profile with the height of the BB peak reflectivity of neighboring LVPRs may help in this regard. It is also hoped that the optimization of the numerous parameters used for the identification of a melting region from polarimetry, or from the reflectivity "LVPRs", and of the snow region from reflectivity gradients may improve the existing algorithm as experienced is gained from examining additional cases. Finally, this research will remain incomplete until validation of its estimates can be made with surface observations and/or with disdrometic data. Additional images and animation not presented here because of manuscript size constraints are available online at: http://132.206.43.159/~aldo/rsbd

7. REFERENCES

Bellon, A., G. Lee, A. Kilambi, and I. Zawadzki, 2007: Real-time comparisons of VPR-corrected daily rainfall estimates with a gauge mesonet. *J. Appl. Meteor.*, **46**, 726-741..

Brandes, E. A., and K. Ikeda, 2004: Freezing-level estimation with polarimetric radar. *J. Appl. Meteor.*, **44**, 1541-1553.

Fabry, F., and I. Zawadzki, 1995: Long-term observations of the melting layer of precipitation and their interpretation. *J. Atmos. Sci.*, **52**, 838-851.

Germann, I., and J. Joss, 2002: Mesobeta profiles to extrapolate radar precipitation measurements above the Alps to the ground level. J. *Appl. Me*teor., **41**, 542-557

Gourley, J. J., and C. M. Calvert, 2003: Automated detection of the bright band using WSR-88D data. *Wea. Forecasting*, **18**, 585-598.

Marshall, J. S., and E. H. Ballantyne, 1975: Weather Surveillance Radar. *J. Appl. Meteor.*, **14**, 1317-1338.

Matrosov, S. Y., K. A. Clark, and D. E. Kingsmill, 2007: A polarimetric radar approach to identify rain, melting-layer, and snow regions for applying corrections to vertical profiles of reflectivity. *J. Appl. Meteor.*, **46**, 154-166.

Meischner, P., V. N. Bringi, M. Hagen, and H. Holler, 1991: Multi-parameter radar characterization of a melting layer compared with in situ measurements. Preprints, *25th Int. Conf. on Radar Meteorology*, Paris, France, Amer. Meteor. Soc., 721-724.

Miller, D. J., and K. A. Scharfenberg, 2003: The use of polarimetric radar data in the winter weather warning decision making system: A case study, Preprints *31st Int. Conf. on Radar Meteorology*, Seattle, WA, Amer. Meteor. Soc.,976-979.

Lee, G., 2006: Sources of errors in rainfall measurements by polarimetric radar: Variability of drop size distributions, observational noise, and variation of relationships between R and polarimetric parameters. *J. Atmos. Oceanic Technol.*, **23**, 1005-1028.

Rogers, R.R., and W. O. J. Brown, 1997: Radar observations of a major industrial fire. *Bull. Amer. Meteor. Soc.*, **78**, 803-814.

Ryzhkov, A. V., and D. S. Zrnic, 1998: Discrimination between rain and snow with a polarimetric radar. *J. Appl. Meteor.*, **37**, 1228-1240.

Ryzhkov, A. V., and D. S. Zrnic, 2003: Discrimination between rain and snow with a polarimetric NEXRAD radar. Preprints, *31st Int. Conf. on Radar Meteorology*, Seattle, WA, Amer. Meteor. Soc., 635-638.

Ryzhkov, A. V., T. J. Schuur, D. W. Burgess, P. L. Heinselman, S. E. Giangrande, and D. S. Zrnic, 2005: The joint polarization experiment. *Bull. Amer. Meteor. Soc.*, **86**, 809-824.

Sanchez-Diezma, R., I. Zawadzki, and D. Sempere-Torres, 2000 : Identification of the bright band through the analysis of volumetric radar data. *J. Geophys. Res*., **105**, 2225-2236.

Scharfenberg, K. A., and E. Maxwell, 2003: Operational use of a hydrometeor classification algorithm to detect the snow melting level. Preprints, *31st Int. Conf. on Radar Meteorology*, Seattle, WA, Amer. Meteor. Soc., 639-641.

Seo, D.-J., J. Breidenbach, R. Fulton, D. Miller and T. O'Bannon, 2000: Real-time adjustment of range-dependent biases in WSR-88D rainfall estimates due to nonuniform vertical profile of reflectivity. *J. Hydrometeor*., **1**, No. 3, 222-240

Stewart, R. E., 1992: Precipitation types in the transition region of winter storms. *Bull. Amer. Meteor. Soc*., **73** 287-296.

Vignal, B., and W. F. Krajewski, 2001: Large-scale evaluation of two methods to correct range-dependent error for WSR-88D rainfall estimates, *J. Hydrometeor*., **2**, 490-504

Vivekanandan, J., D. S. Zrnic, S. M. Ellis, R. Oye, A. V. Ryshkov, and J. M. Straka, 1999: Cloud microphysics retrieval using S-band dual-polarization radar measurements. *Bull. Amer. Meteor. Soc*., **80**, 381-388.

Zawadzki, I., A. Bellon, C. Côté, and F. Fabry, 2001: Target identification by dual-polarization radar in an operational environment. Preprints, *30th Int. Conf. on Radar Meteorology*, Munich, Germany, Amer. Meteor. Soc., 165-167.

Zrnic, D. S., N. Balakrishnan, C. Ziegler, V. Bringi, K. Haydin, and T. Matejka, 1993: Polarimetric signatures in the stratiform region of a mesoscale convective system. *J. Appl. Meteor*., **32**, 678-693.

Zrnic, D. S., and A. V. Ryshkov, 1999: Polarimetry for weather surveillance radars. *Bull. Amer. Meteor. Soc*., **80** , 389-406.